AIAA PAPER
75-6

FLARE-INDUCED SEPARATION LENGTHS IN SUPERSONIC,
TURBULENT BOUNDARY LAYERS

by
A. ROSHKO and G. J. THOMKE
McDonnell Douglas Astronautics Company
El Segundo, California

AIAA PAPER 75-6

AIAA 13th Aerospace Sciences Meeting

PASADENA, CALIF. / JANUARY 20-22, 1975

FLARE-INDUCED SEPARATION LENGTHS IN SUPERSONIC, TURBULENT BOUNDARY LAYERS

A. Roshko* and G. J. Thomke†
McDonnell Douglas Astronautics Company
El Segundo, California

Abstract

Experimental results are presented for the effects of Mach number, Reynolds number, and corner angle on flare-induced separation of a supersonic, turbulent boundary layer. In particular, measurements were obtained for the variation with flare angle, α, of the ratio (ℓ_o/δ_o) of the upstream interaction length to boundary-layer thickness at the beginning of the interaction for Mach numbers $2 \leq M \leq 4.5$, boundary-layer thickness Reynolds numbers $10^5 < R_\delta < 10^6$, and adiabatic wall conditions. The model consisted of a hollow cylinder of 12-in. diameter and 51-in. length. Flares of angle $9° \leq \alpha \leq 40°$ were attached to the cylinder at either of two locations, viz., at x_c = 14 or 28 in. downstream from the sharp leading edge. Measurements consisted chiefly of surface-pressure distributions. Profiles for the undisturbed (flare-off) boundary layer were also obtained. By varying the several parameters, upstream interaction lengths as large as $\ell_o/\delta_o = 30$ were observed. It was found that ℓ_o/δ_o decreases with increasing Mach number and Reynolds number and, of course, increases with flare angle. It was also found that, for constant α, when ℓ_o/δ_o is plotted versus the local undisturbed value for the skin-friction coefficient, C_{f_o}, the Mach-number dependence disappears. From this observation, a simple correlation formula was obtained and used to compare results from other investigations, and also to correlate incipient separation data. The present results complement the incipient-separation data obtained previously by us in the next higher decade of Reynolds number and further confirm the trends established there. It was also found that, for large α, the separated region upstream of the flare has free-interaction characteristics similar to those of upstream-facing steps at high Reynolds number.

Nomenclature

- C_f = $2\tau_w/\rho_e U_e^2$, local skin-friction coefficient
- C_f^* = value of C_f at $\ell_o/\delta_o = 0$
- H = δ^*/θ, boundary-layer shape parameter
- ℓ = interaction length, measured upstream from corner
- M = Mach number
- n = velocity profile parameter, $U/U_e = (y/\delta)^{1/n}$
- P = pressure
- ΔP = $P - P_e$, pressure differential
- r = radius of cylinder outer surface
- R_Δ = $\rho_e U_e \Delta/\mu_e$, Reynolds number based on $\Delta = \delta$, θ, or $c = x_c$
- T = temperature
- U = velocity
- x = distance downstream from leading edge of cylinder
- x_c = distance from leading edge to corner
- y = radial distance from cylinder surface
- α = flare angle, deg
- β = shock-wave angle
- δ = boundary-layer thickness
- δ^* = boundary-layer displacement thickness
- θ = boundary-layer momentum thickness
- μ = viscosity coefficient (Sutherland's formula)
- ξ = wetted distance from compression corner, positive upstream
- ρ = density
- σ = upstream-influence coefficient for a compression corner
- τ = local shear stress
- ϕ = angular coordinate used to specify the circumferential location of a point (x, r, ϕ) on the cylinder surface
- ψ = effective flow turning angle of the free shear layer

Subscripts

- c = undisturbed conditions at compression corner
- D = conditions for shock detachment
- e = free-stream conditions
- F = denotes overall pressure rise on flare
- i = conditions for incipient separation
- o = undisturbed conditions at beginning of interaction
- P = denotes plateau pressure level for large separated regions
- r = recovery conditions
- s = conditions at separation point
- t = free-stream total conditions
- w = conditions at the surface

Introduction

The investigations reported in this paper are a natural development from the earlier work of the authors[1] on incipient separation in supersonic, turbulent boundary layers at very high values of Reynolds number. The authors had found trends quite different from those which could be extrapolated from prior results at lower values. Specifically, we found that in the range of Reynolds number (R_c) based on chord length (x_c) from 10^8 to 10^9, the ramp angle needed to induce separation, α_i, increases with R_c. This is opposite to what had been observed at values of R_c below 10^7 by Kuehn[2] and others. It was natural to ask whether the increased "resistance to separation" at high Reynolds number occurs also for values of ramp angle, α, greater than α_i — that is, for separated flow. Indeed, the few results obtained[1] indicated that the separation length (ℓ_s) upstream of the ramp, normalized by the boundary-layer thickness (δ_o) just ahead of the interaction, decreases with increasing Reynolds number. However, it was not possible in the experimental configuration of Ref. 1 to explore a large range of separation length.

*Consultant; also Professor of Aeronautics, California Institute of Technology. Fellow AIAA.

†Senior Engineer/Scientist, Aerophysics Laboratory. Member AIAA.

Recently, Settles and Bogdonoff[3] measured the upstream interaction length, ℓ_0,† in the range $R_c = 10^7$ to 10^8 and found also that ℓ_0/δ_0 decreases with increasing values of the boundary-layer thickness Reynolds number, R_δ. However, this increased resistance to separation did not occur in the case of incipient separation, for which they found α_i to be insensitive to Reynolds number. On the other hand, Law,[4] working in the same range of Reynolds number and at the same Mach number ($M_e \simeq 3$) as Settles and Bogdonoff, found that with increasing Reynolds number ℓ_0/δ_0 decreases and α_i increases. Also, his data for incipient separation fall on a curve that is a continuation of the results reported in Ref. 1 for the next higher decade of Reynolds number.

Earlier, a semi-empirical method by Kessler and Page [5] had predicted that separation length would decrease with increasing Reynolds number. Their calculations were based on an adaptation of Korst's method. Another calculation, by Hunter and Reeves, [6] using the Lees-Reeves integral method, predicted the same influence of Reynolds number.

Earlier still, the problem of the extent of separation in a turbulent supersonic boundary layer had attracted the attention of many investigators, and various correlations were attempted, but with little success. A difficulty has been the lack of systematic data collection. In a survey of over 100 papers and reports giving experimental results, we found it difficult to sort out trends. The great bulk of the data was in a range of Reynolds number, R_c, from about 10^5 to 10^7, or even narrower — this dictated by the characteristics of the typical small or medium-sized supersonic wind tunnels in which research of this kind was ordinarily conducted. In this range, the flows were transitional more often than not, or had hardly recovered from the effects of transition or tripping, so that the establishment of accurate trends in purely laminar or purely turbulent separation proved difficult. This difficulty was compounded by the facts that any one investigation was usually conducted over a rather limited range (if any) of Mach number and Reynolds number, and different investigators used different ramp angles, usually with little variation. It was therefore difficult, even with interpolation and extrapolation, to put together a broad picture.

In designing the experiments described here, the aim was to take advantage of the high Reynolds-number capability offered by a large wind tunnel so that separation lengths could be varied systematically over as wide a range as possible of the relevant parameters, namely the ramp angle (α), Mach number (M_e), and Reynolds number (R_c or R_δ). It would have been desirable to continue with the experimental arrangement of Ref. 1, where wall boundary-layer thicknesses ranged from 3 to 6 in., but model blockage and shock-wave-induced interference effects would have appreciably diminished the range of α and ℓ_0/δ_0 for which valid data could be obtained. Further study indicated that the desired goals could best be achieved by using a 1-ft-diameter hollow cylinder to which flares of various angles could be attached. Experimental conditions would cover a range of Reynolds number, $R_\delta \simeq 10^6$ to 10^7 — i.e., one decade lower than that of Ref. 1. With a sharp leading edge, supersonic flow through the inlet, and boundary-layer thicknesses small compared to the cylinder radius ($\delta/r < 0.07$), the boundary layer and adjacent flow field would be similar to those for a flat plate. However, for large separation regions ahead of the larger flares, an effect of the axisymmetric parameter x_c/r could be expected.

Advantages of using a large, hollow, axisymmetric model were many. Chief among these were that end effects were eliminated; natural transition occurred well ahead of the flare; supersonic flow through the inlet eliminated both nose effects and interference caused by bow-wave reflections from the tunnel sidewalls; and low-cost configuration changes could easily be effected for (later) studies on the effects of nose shape, transition (including artificial trips), and yaw angle.

Experimental Arrangement and Procedure

Wind Tunnel

The experiment was set up in the 4- by 4-ft Trisonic Wind Tunnel [7] located at the McDonnell Douglas Aerophysics Laboratory in El Segundo, California. This is a blowdown-to-atmosphere wind tunnel that can provide run times from 10 to 100 sec, depending on conditions.

For the experiment, the flexible walls forming the two-dimensional nozzle of the tunnel were set to provide test-section Mach numbers from 2.0 to 4.5. Unit Reynolds number was varied from 0.5 to 2 million per inch at each Mach number by adjusting total pressure. Depending upon Mach number, total temperatures were in the range from 520 to 630° R to prevent air liquefaction and to provide nearly adiabatic wall conditions for the model. During a run, total temperature decreased slightly (no more than 10° over the total run interval, and less than 5° during a data measurement interval).

Model

The basic part of the model, the hollow cylinder, was a steel tube with an outside diameter of 11.94 in. and a wall thickness of 0.34 in. The 51-in. length was comprised of a 5-in. nose (inlet) section followed by a 46-in. instrumented section. The outer surface of the tube was machined and polished to a 32-μin. finish. The inlet section was chamfered internally at an angle of 4° and honed to provide a sharp leading edge. Compression corners were formed on the outer surface of the cylinder by attaching to it two flare halves, separated by splitter plates, as shown in Fig. 1.

The economies that can be realized by using two flare angles per run are obvious. The feasibility of using this arrangement had been studied in some previous, unpublished work

†ℓ_0 is nearly equal to the distance from the corner to the beginning of the surface-pressure rise (see Fig. 5). It is always slightly larger than ℓ_s, and it is more conveniently and consistently determined. Qualitatively, it is not important to distinguish between ℓ_0 and ℓ_s in general discussion.

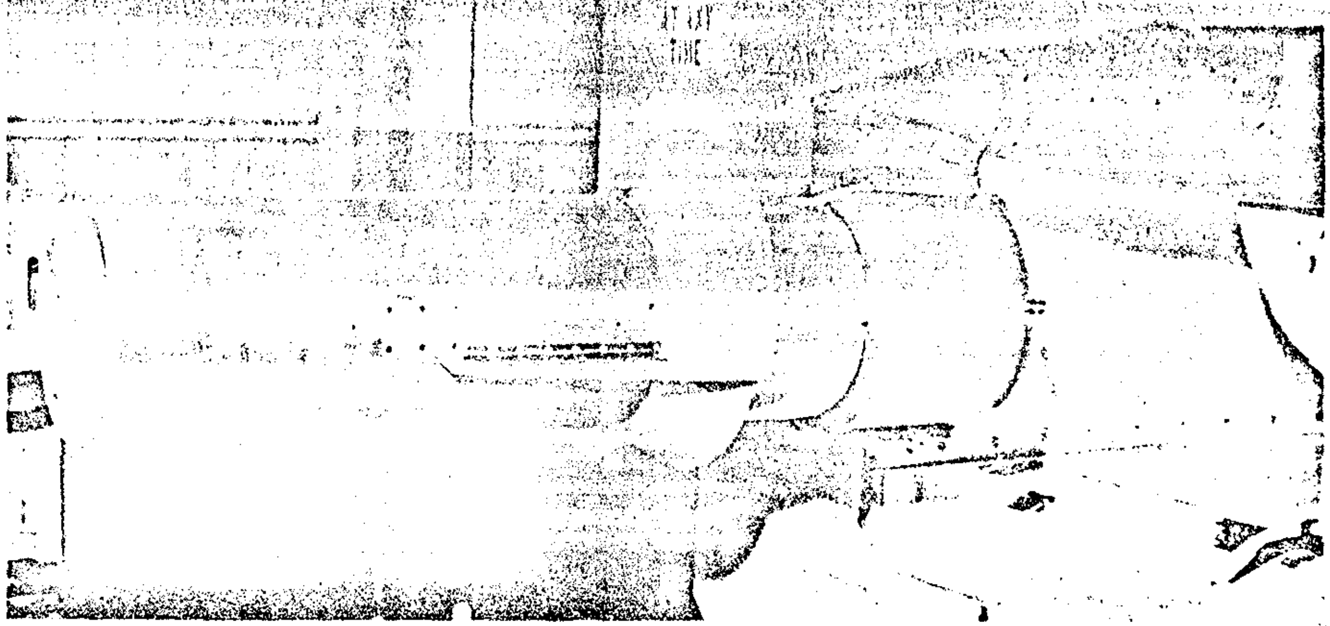

Fig. 1 Model with 40°/30° half-flares at x_c = 28 in.

(related to that in Ref. 8) on an axisymmetric, downstream-facing step, where it was found that splitter plates had practically no effect on the extent of the separated region, even when the circumferential distance between the plates was as small as 45° (compared to 180° in the present case).

In the present experiments, we provided for data comparisons with a full flare at one angle (α = 25°). Flares were made of aluminum and paired according to the following values for α: 9-13, 19-20, 22-25, 25-25 (with and without splitter plates), 27-35, and 30-40°. Slant length ranged from 4.6 in. (α = 13°) to 5.9 in. (α = 40°). Flare pairs could be positioned at two locations on the cylinder, x_c = 14 or 28 in. measured downstream from the leading edge of the cylinder to the leading edge of each flare. Corresponding values of the axisymmetric parameter, x_c/r, are 2.33 and 4.66, respectively. A dowel-pin/bearing-block arrangement prevented flare movement with respect to the cylinder. Flare-to-cylinder contact surfaces were sealed at the base of each flare and along the splitter plates to prevent air leakage from the corner region. Splitter-plate leading edges had a 5° half-angle and were positioned 12 in. ahead of the compression corner for the α = 30-40° pair and 4 in. ahead of the corner for all other α.

The aft section of the cylinder surface was instrumented with 146 orifices (0.03-in. diameter) for sensing surface pressure and a thermocouple for sensing surface temperature. Orifices were arranged in staggered arrays about the leeward (ϕ = 0°) and windward (ϕ = 180°) rays on the cylinder surface between 12 ≤ x ≤ 28 in., and were more densely distributed near x = 14 in. and 28 in. Instrumented flares (α ≤ 25°) had 16 orifices spaced over a 3-in. length measured along the surface downstream from the flare leading edge.

Instrumentation

Sixteen miniature, strain-gauge-type, absolute-pressure transducers having rated capacities of 5 psia or 10 psia were used in conjunction with pressure switches to sense model surface pressures. During one cycle of the pressure switches, each transducer sensed 11 model pressures, three precisely known monitor pressures, and two reference pressures (P_{ref} ≤ 50 μm Hg). Each switch was cycled three times during each run, and data were recorded during each cycle in order to evaluate capillary lag effects, if any. Schlieren photographs were taken during each run to assist in evaluation of test results.

A traversing probe was used to obtain boundary-layer pitot-pressure profiles. The probe tip was formed by flattening and honing a piece of 0.04-in. outside diameter by 0.005-in. wall steel tube to provide a 0.005-in. tip height, 0.002-in. slit height, and a 0.05-in. slit width. The drive unit consisted of a gear train driven by an electric motor. It was housed on the outer surface of the cylinder diametrically opposite the probe. The probe was linked to the drive unit by a thin, diamond-shaped blade that passed through the cylinder walls and duct. Fully retracted, the probe tip lay below the cylinder surface in a specially constructed open recess. Pitot pressure was sensed with a 30-psid transducer located in the drive-unit housing. Probe movement was sensed with an infinite-resolution film potentiometer. All factors being considered, it is estimated that uncertainty in probe position, y, was less than ± 0.002 in.

Analog outputs from all pressure transducers, thermocouples, and the probe position indicator were digitized and recorded on magnetic tape with a computer-controlled, 32-channel, high-speed data-acquisition system.

Procedure

The model was supported in the tunnel as shown in Fig. 1 with the leading edge upstream of the tunnel Schlieren window. During the experiment, the centerline of the cylinder was held coincident with the tunnel test-section centerline. Comparisons made between surface-pressure distributions at $\phi = 0°$ and $180°$ confirm that the model was aligned parallel to the tunnel flow.

Pitot-pressure surveys of the boundary layer plus measured surface-pressure distributions indicate that the strength of the wave emanating from the model leading edge was negligibly small for all free-stream test conditions. This and other measurements indicate that the flow through the cylinder inlet was always supersonic.

The flare experiments were run at nominal Mach numbers of 2, 2.5, 3, 3.3, 3.5, 3.7, 4, and 4.5, and at tunnel unit Reynolds numbers of 0.5, 1.0, 1.5, and 2.0 million per inch. Thus, an eightfold change in length Reynolds number, R_c, was possible. Wall-temperature to recovery-temperature ratios for the model were in the range $0.95 \leq T_W/T_r \leq 1.05$. During a run, Mach number, Reynolds number, and flare angle were constant. For each run, data were recorded, reduced to engineering units, and plotted "on line." On-line examination of the data was useful for selecting conditions for later runs.

Data repeatability and model alignment were evaluated for M = 2, 2.5, and 3 using the $\alpha = 25\text{-}25°$ flare pair positioned at $x_c = 28$ in. For each value of M, comparisons were made first between results obtained during a run for individual flare halves, and second between data from repeat runs. These comparisons show that data repeatability was excellent and further confirm that the model was aligned parallel to the tunnel flow.

Splitter-plate effects were evaluated at $M = 2.5$ ($\ell_o/\delta_o = 4$) by comparing results obtained at $x_c = 28$ in. for the $\alpha = 25\text{-}25°$ pair with and without plates. A similar evaluation was made at M = 3 by comparing data for the $\alpha = 25\text{-}25°$ pair (without plates) with data for the $\alpha = 22\text{-}25°$ pair (with plates). For each case, splitter-plate effects could not be detected. It would have been of interest to study plate effects for larger flare angles, say $\alpha = 40°$, where values for the interaction-length to circumferential-span ratio, $\ell_o/\pi r$, ranged between 0.3 and 0.5, but this was not done.

Pitot-pressure profiles for the undisturbed (flares-off) boundary layer on the cylinder were obtained at x = 14 and 28 in. for the ranges of Mach number and Reynolds number covered in this study, viz., $2 \leq M \leq 4.5$ and $7 \times 10^6 \leq R_c \leq 60 \times 10^6$. At these locations, representative values of the boundary-layer thickness were $\delta = 0.195$ and 0.355 in., corresponding to values of the boundary-layer-thickness to cylinder-radius ratio, $\delta/r = 0.03$ and 0.06.

Boundary-layer trip devices were not employed. According to data presented by Pate and Schueler, (9) the position of natural transition on the cylinder was estimated to be from 2 to 8 in. from the leading edge, depending on M and R_c.

Results

The experimental results consisted principally of the various parameters describing the undisturbed boundary layer on the cylinder, Schlieren photographs of the interaction region, and surface-pressure distributions.

Boundary-Layer Parameters

Boundary-layer Mach-number profiles were computed from the measured pitot-pressure values, not corrected for probe displacement effects, with wall pressure assumed to be constant through the layer. Velocity and density profiles were calculated assuming the temperature profile to be given by

$$T/T_e = T_w/T_e + (T_r/T_e - T_w/T_e)(U/U_e) - (T_r/T_e - 1)(U/U_e)^2 \quad (1)$$

By making the following substitutions in Eq. (1),

$$U/U_e = (M/M_e)(T/T_e)^{1/2}$$

$$T_w/T_e = (T_w/T_t)(1 + 0.2M_e^2)$$

$$T_r/T_e = 1 + 0.178M_e^2$$

one arrives at a quadratic equation solvable for $(T/T_e)^{1/2}$ in terms of T_w, T_t, M_e, and M/M_e.

The outer portion of the velocity profile was assumed to be represented by a $1/n$-type power law, and n was taken to be equal to the slope of the best straight-line fit to logarithmic values of y and U/U_e for $y > 0.03$ in. Values for n ranged from 5.5 to 6.5 at $x_c = 14$ in. and 6.0 to 7.5 at $x_c = 28$ in.

Because the velocity ratio, U/U_e, asymptotically approaches a value of 1.0 for values of $y \doteq \delta$, the determination of precise values for δ is difficult and somewhat arbitrary. We chose for δ the value of y at $U/U_e = 0.995$. The curves of Fig. 2 represent the smoothed values of δ_c obtained for the undisturbed boundary layer at $x_c = 14$ and 28 in. for the range of Mach number and (unit) Reynolds number shown. Data scatter about each curve is less than 3%. These results indicate that dependence on Mach number is small and decreases with increasing Reynolds number. It might have been better to display the results in terms of a Reynolds number based on the distance from the transition point instead of the leading edge, but this was not done because no attempt was made to determine the location of transition experimentally. This would have shown the Mach-number dependence to be even less than in Fig. 2 because the transition point moves downstream with increasing Mach number. (9)

The momentum deficit thickness was determined by graphically integrating the expression

$$\theta = \int_0^\infty (\rho U/\rho_e U_e)\,[1 - (U/U_e)]\,dy$$

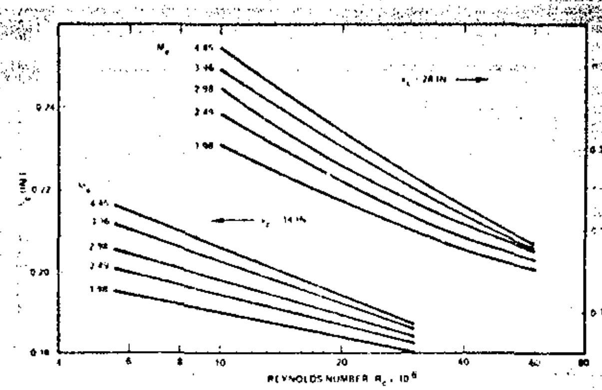

Fig 2 Boundary-layer thickness at x_c = 14 and 28 in.

Values obtained for θ_c are plotted in Fig. 3. To scale the thickness parameters to values of x other than x_c = 14 and 28 in., use was made of the following equations:*

$$\delta/x = 0.1215\, R_x^{-1/8} \qquad (2)$$

$$\theta/x = 0.0125\, e^{-M/5}\, R_x^{-1/8} \qquad (3)$$

The scaling procedure consists of entering Figs. 2 and 3 with given values of R_c and M_e to obtain δ_c and θ_c. Values for δ_o and θ_o at the beginning of the interaction, i.e., at $x_o = x_c - \ell_o$, were calculated from Eqs. (2) and (3):

$$(\delta_o/\delta_c) = (\theta_o/\theta_c) = (x_o/x_c)^{7/8}$$

All values for the local skin-friction coefficient, C_f, used in this paper were obtained from the equations of Hopkins[10] based on the method (II) of Van Driest, into which were put measured or estimated values for M_e, T_t, and R_θ plus the adiabatic wall condition, $T_w/T_r = 1$. Sutherland's formula for viscosity was also used. We note that values of C_f computed from Eq. (3) and $C_f = 2d\theta/dx$ are within 10% of the values computed from the equations of Ref. 10.

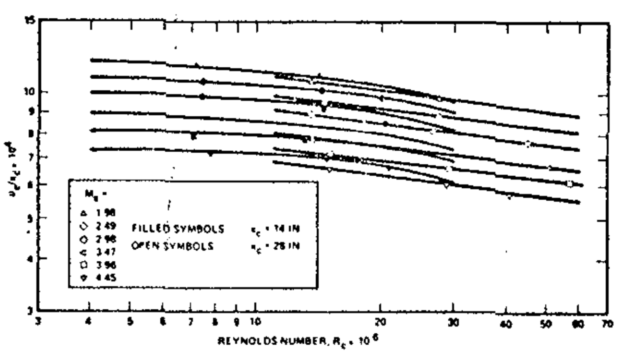

Fig 3 Momentum thickness at x_c = 14 and 28 in.

Flow Visualization

Figure 4 is a Schlieren photograph obtained during the study for x_c = 14 in. at M_e = 2.98. Clearly visible for the upper (α = 40°) flare are the separation shock emanating from the beginning of the interaction region, the outer edge of the free shear layer, the flow reattachment region, and the interaction between the separation and reattachment shocks. The weak waves emanating from the cylinder surface upstream of the interaction run along Mach lines having their origins at the cylinder leading edge and the parting line between the two sections of the cylinder. The weak disturbances observed as waves emanating from the tunnel walls are due to the leading edge of a newly applied coat of paint on the test-section walls.

The wave angle, β_s, for the separation shocks observed for both the α = 30° and 40° flares is $\beta_s \simeq 30°$, a result consistent with the free-interaction concept. The outer edge of the shear layer makes a 17° angle with the cylinder. The measured plateau pressure was $P_p/P_e \simeq 2.57$, which corresponds to a two-dimensional inviscid turn of the flow through ψ_s = 13.6°. The 3.4° difference between ψ_s and the outer edge of the layer is in agreement with the values of 3.0 and 3.5° found for the free shear layer ahead of forward-facing steps by Behrens[11] and Zukoski,[12] respectively.

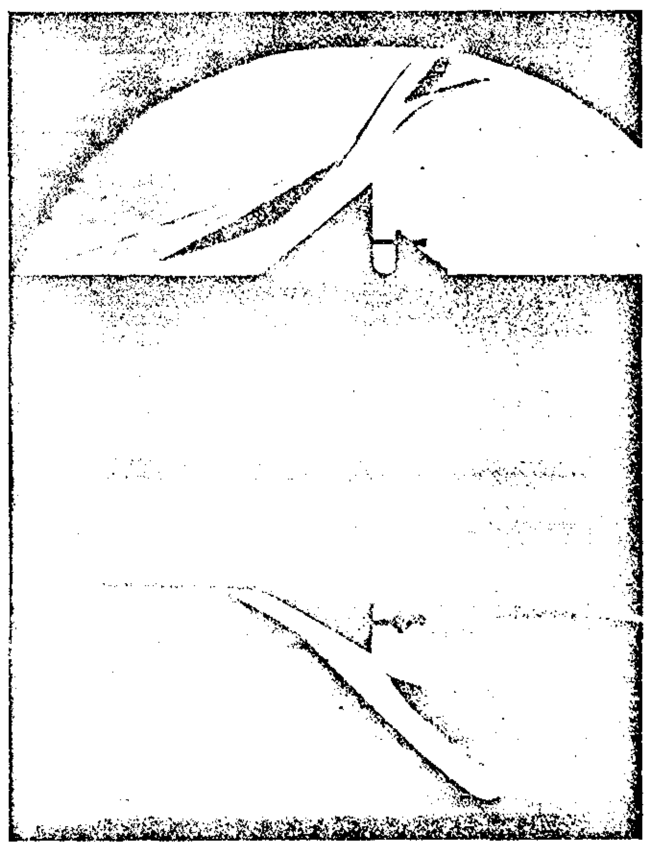

Fig 4 Schlieren photograph (M_e = 2.98, R_c = 5.9 x 10^6, x_c = 14 in., α = 40°/30°

*These, and the equation $\delta^*/x = 0.0163\, e^{M/4}\, R_x^{-1/8}$, are empirical fits that we have made to a large body of experimental results obtained by us, but as yet unpublished, for an adiabatic, flat-plate boundary layer at $10^5 \le R_\delta \le 10^7$ and $1.8 \le M \le 5$. From these, $H = 1.307\, e^{0.45M}$.

The reattachment compression region appears to be about two-thirds of the way up the $\alpha = 40°$ flare surface. It is interesting to note that $\alpha = 40°$ is close to the shock-wave detachment value, $\alpha_D \approx 41°$ for $M_e = 2.98$, assuming a two-dimensional, inviscid, initial turn of the flow through $\psi_s = 13.6°$.

The distance from the corner to the point where the separation shock intersects the surface is a measure of the separation length, ℓ_s. Values for ℓ_s determined from Schlieren photographs are in agreement with, but slightly less than, values of ℓ_o determined from surface-pressure data (definition of ℓ_o is discussed below). This observation agrees with the findings of Law[4] and Spaid and Frishett.[13] Measurements from Fig. 4 indicate values of $\ell_s/x_c = 0.089$ and 0.367 for $\alpha = 30°$ and $40°$, respectively; corresponding surface-pressure data indicate a value of $\ell_o/x_c = 0.094$ for $\alpha = 30°$. (Since pressure orifices were not located upstream of x = 12 in., the beginning of the pressure rise could not be detected for $\alpha = 40°$ at $x_c = 14$ in.) Hereafter we present only measurements of ℓ_o (from pressure distributions), which could be more accurately determined than measurements of ℓ_s (from Schlieren photographs).

Pressure Distributions

An example of a measured pressure distribution is shown in Fig. 5. For this case, $\alpha = 25°$, pressure measurements were obtained on the flare surface as well as the cylinder surface upstream of it. Flares of larger angle were not provided with pressure taps. The method of defining the upstream interaction length, ℓ_o, illustrated in Fig. 5, is the one used by Settles and Bogdonoff.[3]

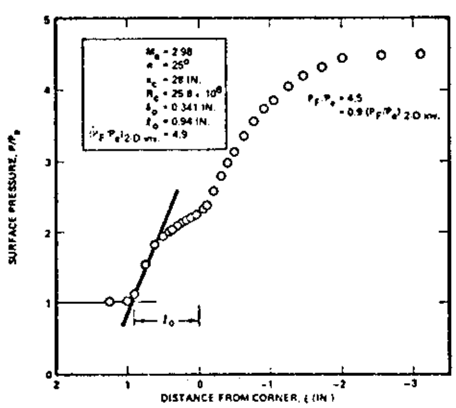

Fig 5 Definition of interaction length

Figure 6 presents a set of pressure distributions obtained at $M_e = 3.96$ for a nominal Reynolds number, $R_c = 30 \times 10^6$. It should be noted that the listed values of C_{fo} are computed for the point at the beginning of interaction and that distances from the corner, ξ, are normalized with the boundary-layer thickness, δ_o, at the beginning of interaction. For $\alpha = 40°$, the interaction begins at $\xi/\delta_o = 25.4$, so only the portion of the pressure distribution closer to the corner is visible in Fig. 6. The nearly constant pressure in this portion is taken to be the plateau pressure, $P_p = 3.12\ P_e$, for this Mach number, $M_e = 3.96$.

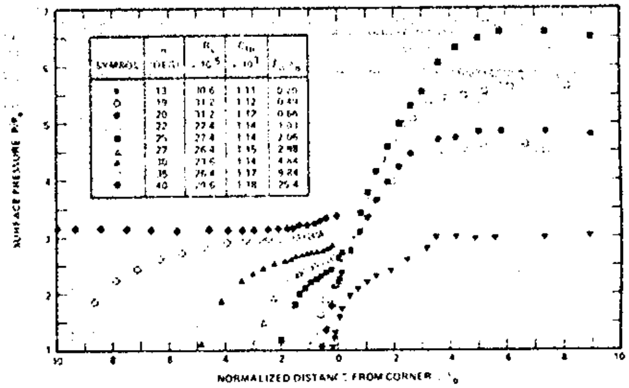

Fig 6 Surface-pressure distributions, $M_e = 3.96$, $x_c = 28$ in.

The values of plateau pressures obtained at the Mach numbers of this experiment are close to those for upstream-facing steps, as shown by the comparison in Fig. 7 with the correlations of Zukoski[12] and of Werle;[14] they were found to be insensitive to Reynolds numbers, as Zukoski had found earlier. Another interesting result is that, for a given Mach number, the plateau pressures at $x_c = 14$ in. and 28 in. are indistinguishable on this plot. That there is no effect of the axisymmetric parameter x_c/r implies that the plateau pressure is determined largely by conditions at separation.

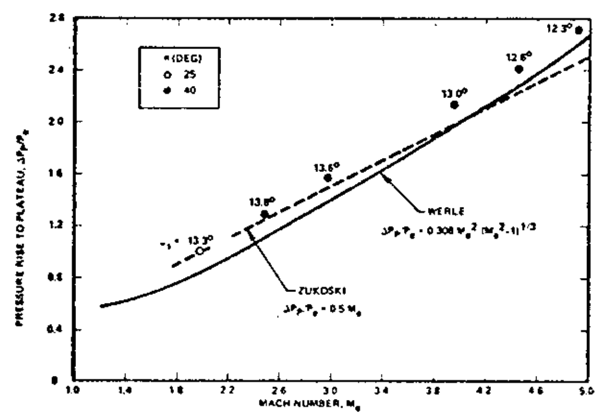

Fig 7 Measured plateau pressures

Interaction Length

The upstream interaction length, ℓ_o, defined as in Fig. 5, was determined for each pressure distribution. The complete set of values over the range of all the parameters is presented in Figs. 8 and 9, in which the interaction lengths have been normalized by x_c, the downstream distance to the flare, and plotted against R_c, the Reynolds number based on x_c. While the trends shown in these basic data plots are interesting, a more significant plot would be based on boundary-layer thickness instead of x_c. It was found, for example, that ℓ_o/Δ ($\Delta = \delta$, δ^*, or θ) decreases with increasing R_Δ, whether Δ be evaluated at x_o or x_c, for the whole range of flow parameters. This is similar to the trends found by Settles and Bogdonoff[3] and by Law[4] at $M \approx 3$ for $\Delta = \delta$. However, we do not show these plots here because, in searching

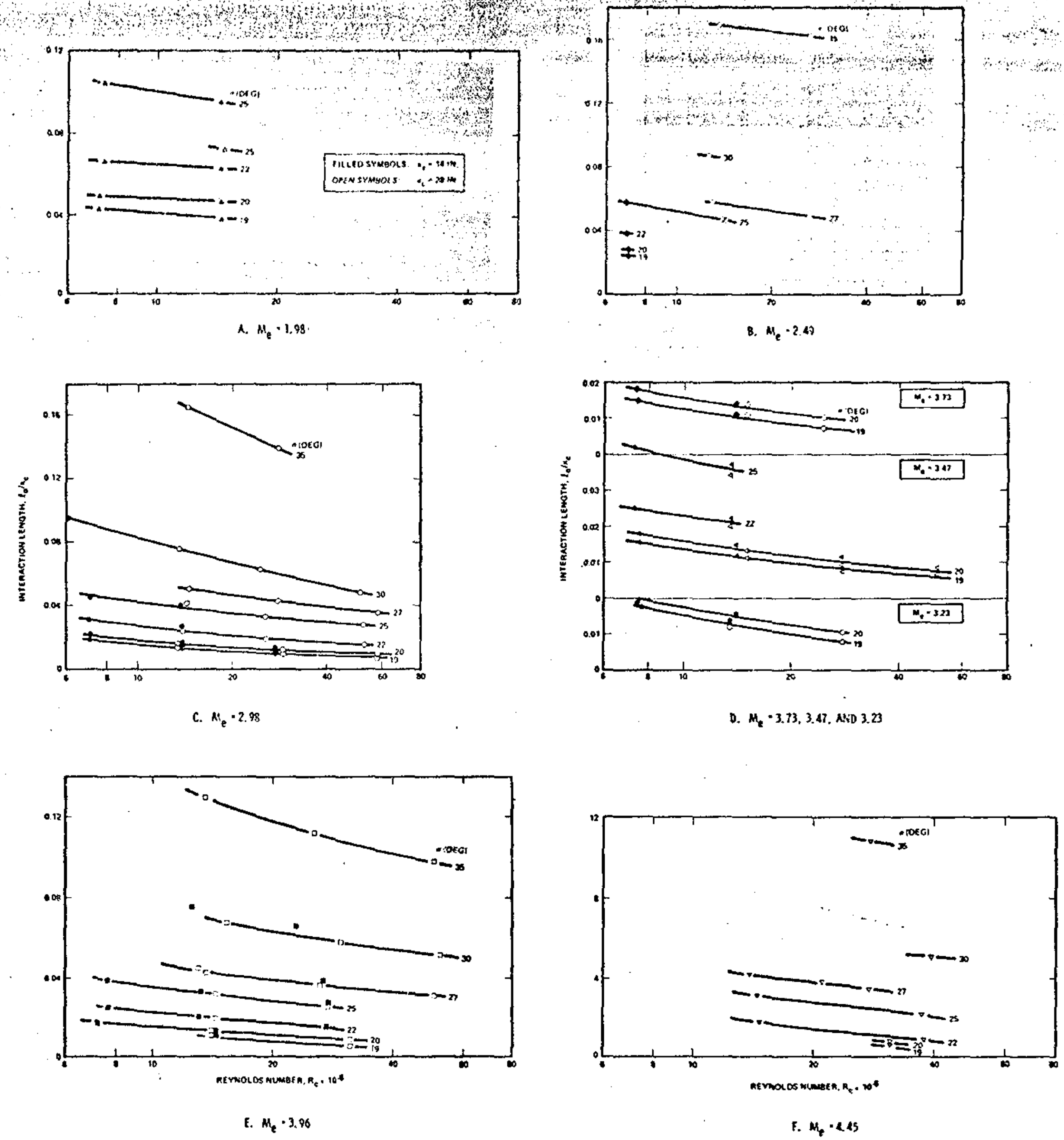

Fig 8 Effect of flare angle and Reynolds number on interaction length

for possible correlations, we came upon a better way to present the data, one in which the dependence on Mach number disappears.

For reasons which we do not yet understand, when l_o/δ_o is plotted against C_{fo}, the data for different values of Mach number (excluding the M_e = 1.98 data) fall onto a single curve for each value of α, as may be seen in Fig. 10. All values of C_{fo} were determined as explained above. The data from the present experiments are in the range $10^5 < R_\delta < 10^6$, but included on the plots are data in the next higher decade, from our previous study.(1, 15) These also fall onto the correlation.

It is remarkable that the data for values of $\alpha \leq 30°$ (and excluding those for M_e = 1.98) fall on a straight line, whose slope we denote by σ. For α = 35°, we have taken some liberty in fitting a straight line to part of the correlation [see remarks following Eq. (6), below]. A discussion of possible factors contributing to the behavior exhibited by the data obtained for M_e = 1.98 and for $\alpha \geq 35°$ is given below. Data for α = 9° and 13° are not included in Fig. 8 and Fig. 10 because only a few data points were obtained, and also because of the difficulty (due to orifice spacing) in obtaining precise values of l_o from surface-pressure measurements for small α. However, four data points

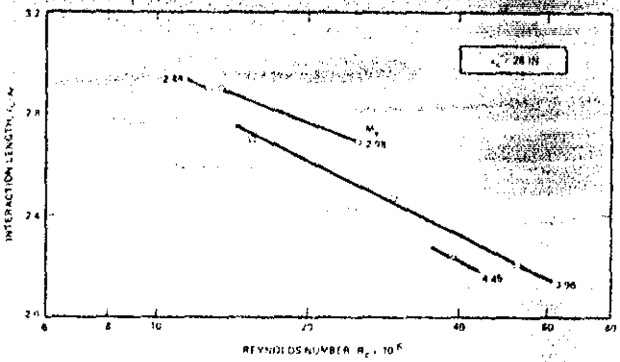

Fig 9 Interaction length for α = 40°

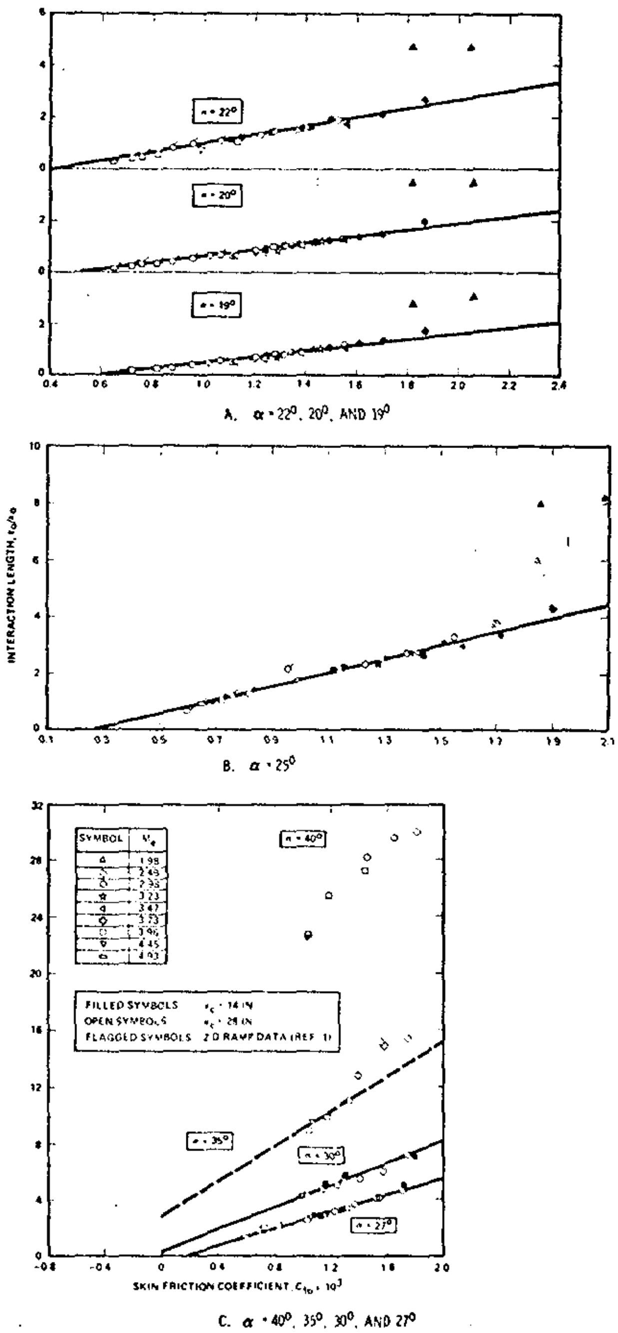

Fig 10 Correlation of upstream influence with local skin-friction coefficient

obtained for $\alpha = 13°$, $x_c = 28$ in., and $M_e = 2.98$ and 3.96, when plotted in the format of Fig. 10, were in agreement with a straight line passing through $C_{fo} = 0.0008$ with slope $\sigma = 400$.

Extrapolation to $\ell_o/\delta_o = 0$ of the straight lines for each α in Fig. 10 defines a parameter, C^*_{fo}, which (formally) is the value of C_f below which the upstream interaction length vanishes. A plot of C^*_{fo} against α, shown in Fig. 11, defines a curve to which the equation

$$C^*_{fo} = 10^{-3}(1 - 0.001189\alpha^2) \tag{4}$$

provides a good empirical fit. The implication of this curve is that for each α, the interaction length becomes zero at sufficiently high Reynolds number ($C_{fo} \leq C^*_{fo}$). However, for $\alpha > 29°$, there is always an upstream influence, no matter how high the Reynolds number.

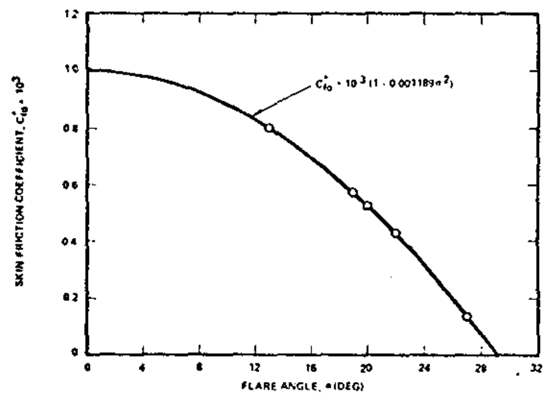

Fig 11 Conditions for zero upstream influence

It is not clear what physical significance, if any, to attach to the extrapolation of the curve for $\alpha < 13°$, particularly the intercept at $\alpha = 0$.

The straight-line used to fit portions of the data in Fig. 10 may be represented by the equation

$$\ell_o/\delta_o = \sigma(C_{fo} - C^*_{fo}) \tag{5}$$

in which, in addition to the parameter $C^*_{fo}(\alpha)$, there appears the upstream influence coefficient, σ (i.e., the slope of the line). The values of $\sigma(\alpha)$ are plotted in Fig. 12, along with the empirical equation

$$\sigma = 10^3(\alpha/18.29)^{2.81} \tag{6}$$

which has been fitted to it. This curve defines for $\alpha = 35°$ a value of σ which was used *a posteriori* to fit the data in Fig. 10.

Whatever the physical significance of the parameters C^*_{fo} and σ defined in this way, Eq. (5) can be used to define the interaction length as a function of α and C_{fo}. Such a plot is given in Fig. 13 for flare angles up to 30° and for values of $C_{fo} \leq 0.003$. Higher values of C_{fo} would be in the transition range of Reynolds number for the applicable range of Mach numbers $2.5 \leq M_e \leq 5$. In fact, the correlation should be used with caution for $C_{fo} \geq 0.002$, which was the largest value in the present experiments. Over the range of data from which Fig. 13 was derived, there is no effect of the axisymmetric parameter

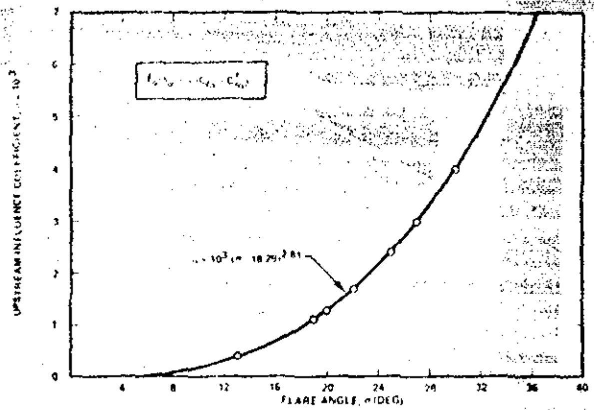

Fig 12 Effect of flare angle on growth rate

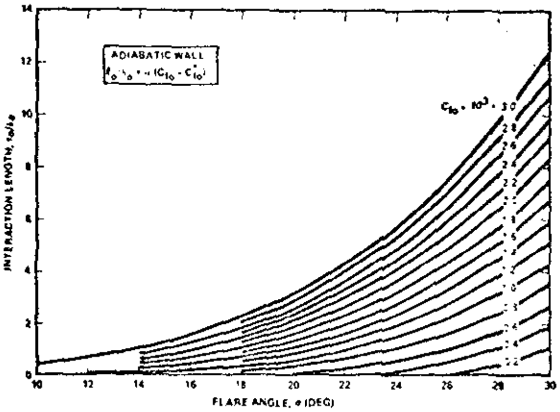

Fig 13 Upstream influence due to a flare ($2.5 \leq M_e \leq 5.0$)

x_c/r (cf. Fig. 10 for x_c = 14 and 28 in., respectively). It is concluded, therefore, that the correlation in Fig. 13 is applicable to two-dimensional flow over a ramp.

In Fig. 14, the correlation is compared with the results of the experiments of Law(4, 16) on a two-dimensional (flat-plate/ramp) configuration and those of Settles and Bogdonoff(3) on an axisymmetric (ogive-cylinder/flare) model for which the axisymmetric parameter x_c/r had the value 14. Both investigations were at $M_e \simeq 3$ in a range of Reynolds number $10^5 \leq R_\ell \leq 10^6$, comparable to that of the present study. Values of C_{f_0} tabulated in the boxes were calculated as described above, using data provided by the authors(3, 16) and with the assumption $T_w/T_r = 1$.

The excellent agreement with part of Law's data and disagreement (up to 20%) with other parts is difficult to reconcile. Apart from quantitative differences, there are curiously abrupt changes in trend (as compared to the smooth correlation curves) at about $\alpha = 22°$. The data of Settles and Bogdonoff agree best with our correlation at about $\alpha = 20°$. For higher values of α, their smaller values of ℓ_0/δ_0 may be due to axisymmetric effect, but the opposite direction for the difference at low α cannot be rationalized. To sum up, the comparison between our data (as represented by the correlation) and that of the other two investigations is not entirely satisfactory.

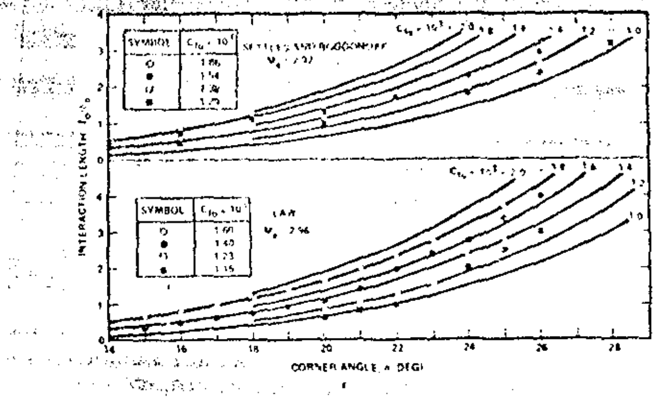

Fig 14 Comparisons between present correlation and experimental results of others ($R_\delta > 10^5$)

Incipient Separation

As mentioned in the introduction, there has been some disagreement about the effect of Reynolds number on the value of ramp angle for incipient separation. Indeed, there has been controversy(13, 17) about even the operational definition of incipient separation conditions. Some of the points of difference are illustrated in the traditional plot (Fig. 15) of incipient separation angle, α_i, against Reynolds number, R_δ, for adiabatic wall conditions. The largest differences occur at the lower end of the Reynolds-number range (10^4 to 10^5). To what extent these differences are due to the different methods of defining separation or to possible differences in boundary-layer properties connected with tripping, etc., has never been satisfactorily settled. In the next higher decade of Reynolds number, there is general agreement between the results of Law(4) and those of Settles and Bogdonoff,(3) but the latter find no dependence on Reynolds number. In the next higher decade, there is only one set of data.(1) Apart from the data of Kuehn, the trends in Fig. 15 are for increasing values of α_i with increasing Reynolds number, i.e., decreasing skin-friction coefficient.

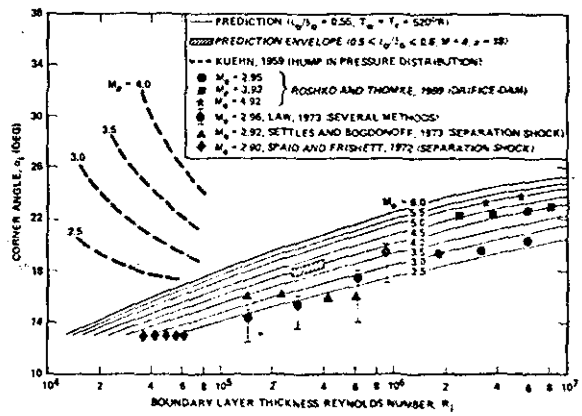

Fig 15 Conditions for incipient separation (traditional plot)

The present experiments were not designed to include detailed measurements of incipient separation. Nevertheless, we hoped to obtain some further data on this question. Our approach to this problem changed considerably after discovery of the Mach-number-independent correlation of Fig. 10. Because the separation point is downstream of the beginning of the interaction ($\ell_s < \ell_o$), it is evident that each straight line in Fig. 10 passes through a value of $\ell_o/\delta_o > 0$ that corresponds to incipient separation ($\ell_s \to 0$). This value of ℓ_o/δ_o for incipient separation may depend on the parameters of the problem, but an examination of our pressure distributions from the present work and from Ref. 1 suggested that in fact it may be relatively constant. Accordingly, we arbitrarily selected, by trial, the value

$$(\ell_o/\delta_o)_i = 0.55 \tag{7}$$

as a definition of incipient separation, independent of Mach number and Reynolds number. In Fig. 10, the intersection of $\ell_o/\delta_o = 0.55$ with the straight-line correlation curves defines corresponding values of α_i and C_{f_i} [these may also be evaluated directly using Eq. (5)]. The result is shown in Fig. 16, where the curve so determined is compared with the data (except Kuehn's) from Fig. 15. Additional results from Refs. 13 and 17, based on different criteria for incipient separation, are also shown. The definition of incipient separation based on the liquid-line technique would correspond to $\ell_o/\delta_o = 0.05$ in the present approach. It may be remarked that values of α_i at lower Reynolds numbers that are based on the pressure-hump technique imply values of $(\ell_o/\delta_o)_i$ larger than unity (as large as 3 for some of Kuehn's data), while at higher Reynolds number, the values of $(\ell_o/\delta_o)_i$ obtained from the pressure-hump technique are in agreement with Eq. (7).

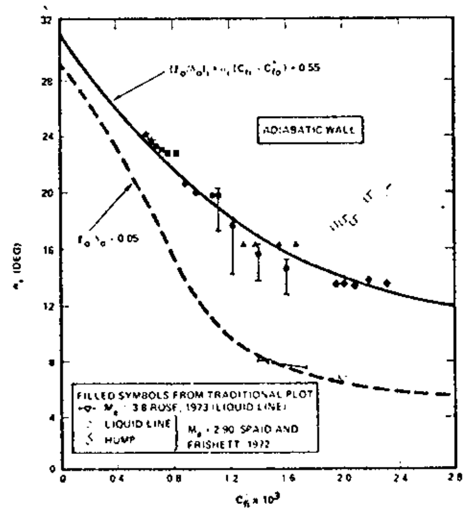

Fig 16 Conditions for incipient separation, $2.5 \le M_e \le 5$ (present correlation)

When the curve defined by Eq. (7) is reinterpreted in terms of the parameters of Fig. 15, it plots as the series of curves shown there. The correlation with most of the data seems to be at least as good as the agreement among the different data. Also shown in Fig. 15 is a measure of the shift in the correlation curves that would occur if the criterion for $(\ell_o/\delta_o)_i$ varied from 0.5 to 0.6.

Discussion

Possibly the most remarkable feature of the results presented above is the disappearance of the Mach-number dependence (for $M_e \geq 2.5$) of the interaction length and of the incipient-separation angle when they are plotted against the skin-friction coefficient. Although the correlation was accidently found by looking for possible correlations with law-of-the-wall parameters, it is not possible to rationalize it in those terms. As we have previously noted,[1] the interaction of a supersonic, turbulent boundary layer with a corner seems rather to be controlled by a wall interaction layer that is considerably thicker than the sublayer and penetrates some distance into the supersonic portion. Similar proposals were made by Rose, et al.[18] and Elfstrom.[19] In fact, Elfstrom incorporated this idea into a method for computing incipient-separation conditions. Increasing Reynolds number, i.e., decreasing C_f, "fills out" the velocity profile and brings the supersonic portion closer to the wall (relative to δ), reducing the wall-layer thickness and the related scale of the interaction. It is this effect that controls both the conditions for incipient separation and the interaction length, ℓ_o. When the external Mach number is too low ($M_e < 2$), the Mach number at the edge of the interaction layer is low enough that the interaction becomes a "transonic" one with rather different characteristics from those at higher Mach numbers. We had noted this in the experiments of Ref. 1. For example, at $M_e = 1.95$, the shock wave ahead of the corner was detached, even for values of α for which the boundary layer had not yet separated. We believe that the fact that the present $M_e = 1.98$ data do not fall on the correlation curves in Fig. 10 may be connected with such "transonic" behavior. In passing, we note that the $M_e \simeq 2$ data from Ref. 1 and from the present experiments consistently fall onto values of "effective α" about 4° above those for the correlation curves in Fig. 10.

To obtain a clearer understanding of these interactions requires a rational understanding of how the thickness of the postulated wall interaction layer is determined. Our own and others' (18), (19) methods for defining it have been ad hoc. Explanations for the Mach-number independence in Fig. 10 and for the linear dependence on C_f await a better understanding of the "wall interaction layer."

As regards the experimental data themselves, we noted in the introduction that until very recently there was very little information available on separation lengths in fully developed turbulent boundary layers. Now that this situation has been somewhat remedied by the work reported in Refs. 3 and 4 and the present paper, it is annoying to find more disagreement than would seem to be warranted. Axisymmetric effects (especially in Ref. 3) may account for some of the differences in interaction lengths at the higher values of α, but they should not be important for incipient separation. The same may be said in regard to sidewall or end effects, which may have played a role in the two-dimensional experiments of Ref. 4 and possibly in our own use of splitter plates. Again, for incipient separation, those effects should not be important.

Still another factor may be wall temperature, i.e., the parameter T_w/T_r. It is known that separation lengths are sensitive to this. An important point in this regard is that the present correlation is strictly for the adiabatic condition, $T_w = T_r$. The plot of ℓ_o/δ_o against C_f (Fig. 10) does not apply for $T_w \neq T_r$, even if the effects of heat transfer on C_f are taken into account. For example, the effect of wall cooling ($T_w < T_r$) is to increase C_f; the present correlation would predict a corresponding increase in ℓ_o/δ_o when, in fact, a decrease is observed.[13] The probable explanation is that wall cooling makes the velocity profile fuller and reduces the thickness of the wall interaction layer. In the present experiments, we saw evidence of these wall-temperature effects in Schlieren photographs taken immediately after the tunnel started at the time the total-temperature transient peaked. However, the data reported here and used in the correlations were obtained under stable, nearly constant total-temperature conditions for which the wall temperature was within 5% of the calculated recovery temperature.

With respect to the results for values of α greater than 30° it may be seen from Fig. 10 that Mach-number independence still exists for $\alpha = 35°$ and 40°. However, these data are not included in the correlation plot of Fig. 13 for several reasons. First, they do not fall so evidently onto straight-line correlations (as explained earlier, the straight line shown for $\alpha = 35°$ was obtained "after the fact"). It is also noted that these values of α are large enough that the angles through which the separated, reattaching shear layers must turn are approaching the maximum values possible[20] and even the maximum values possible for turning without shock detachment. Under these conditions, the reattachment point may be expected to move rapidly downstream (with increasing α), and the separation point correspondingly upstream. When the reattachment point reaches the shoulder, the flow would be basically the same as that ahead of a step, and the separation point would have reached a distance 4.2 step heights upstream of the shoulder.[12] In none of the data reported here had this condition yet been reached. For these larger values of α and the correspondingly larger separated region, one might expect an important effect of the axial symmetry. On the other hand, the basically two-dimensional nature of the free-interaction region, described earlier in the discussion of Fig. 7, implies that for a step ($\alpha = 90°$) the upstream interaction distance would be the same as in two-dimensional flow, and one is tempted to conclude that there may not be much effect of axial symmetry for any α. Against this notion is the experience reported in Ref. 20 where, for a spike-cone configuration, angles of reattachment onto the conical surface were observed to be significantly higher than in corresponding two-dimensional flow, implying that for the axisymmetric case, with free-interaction conditions and large separation, the separation region should be smaller than in two-dimensional flow. As mentioned above, such a trend is also suggested by the data of Settles and Bogdonoff.

There remains the vexing question as to the differences in the incipient separation data reported by different investigators, and even by individual investigators who have applied more than one criterion for defining incipient separation. These differences are most pronounced at the lower values of Reynolds number ($R_\delta < 10^5$) where, it may be noted, viscous sublayer thicknesses are a few (up to 10) percent of the boundary-layer thickness. The effect of the sublayer on the pressure distribution is then much greater than at higher values of Reynolds number and Mach number. For example, at large R_δ, the surface-pressure distribution rises steeply from the beginning of interaction (Fig. 6), while at lower R_δ there is more of an upstream "precursor" (e.g., Refs. 2, 13, and 19). In the most recent contribution to this subject, Appels[21] suggests that separation occurs in two steps. The very first separation, as detected by liquid flow, affects only the sublayer, while larger separation involves more of the boundary layer. He thus defines and measures two values of α_i based on "small" and "large" involvement. The measured values* from the "large" criterion agree very well with our correlation curve for $(\ell_o/\delta_o)_i = 0.55$ in Fig. 16, while those from the "small" criterion lie close to the curve for $(\ell_o/\delta_o)_i = 0.05$. Appels' experiments were conducted at values of $M_e = 3.46$ and 5.45, and $10^5 \leq R_\delta \leq 10^6$.

Except for Appels' data for $M_e = 5.45$, the incipient separation data obtained by other investigators (Refs. 19 and 22 to 26) at high Mach numbers ($M > 5$) do not fall onto the correlation in Fig. 16. Even in the Reynolds-number range $10^5 \leq R_\delta \leq 10^6$, they all show the trend of decreasing α_i with increasing R_δ (decreasing C_f). This trend might be interpreted as being due to a shifting of strong sublayer effects to higher Reynolds numbers because of the higher values of Mach number. Those high-Mach-number data have all been obtained on nonadiabatic walls ($T_w < T_r$); therefore, it is not appropriate to include them in Fig. 16, as noted previously in this discussion.

References

1. Roshko, A. and Thomke, G. J., "Supersonic, Turbulent Boundary-Layer Interaction with a Compression Corner at Very High Reynolds Number," Proceedings of the Symposium on Viscous Interaction Phenomena in Supersonic and Hypersonic Flow, USAF Aerospace Research Laboratories, Wright-Patterson Air Force Base, Ohio, University of Dayton Press, May 1969, pp. 109-138.

2. Kuehn, D. M., "Experimental Investigation of the Pressure Rise Required for the Incipient Separation of Turbulent Boundary Layers in Two-Dimensional Supersonic Flow," Memo 1-21-59A, NASA Ames Research Center, Moffett Field, California, Feb. 1959.

*Reference 21 came to our attention too late for the data to be included in our plots.

3. Settles, G. S. and Bogdonoff, S. M., "Separation of a Supersonic Turbulent Boundary Layer at Moderate to High Reynolds Number," AIAA Paper 73-666, presented at the AIAA 6th Fluid and Plasma Dynamics Conference, Palm Springs, California, July 1973.

4. Law, C. H., "Supersonic, Turbulent Boundary Layer Separation Measurements at Reynolds Numbers of 10^7 to 10^8," AIAA Paper 73-665, presented at the AIAA 6th Fluid and Plasma Dynamics Conference, Palm Springs, California, July 1973; also, AIAA Journal, Vol. 12, No. 6, June 1974, pp. 794-797.

5. Kessler, T. J. and Page, R. H., "Supersonic Turbulent Boundary Layer Separation Ahead of a Wedge," 10th Mid-western Mechanics Conference, Developments in Mechanics, Vol. 4, Colorado State University, Aug. 1967, pp. 1011-1028.

6. Hunter, L. G. and Reeves, B. L., "Results of a Strong Interaction, Wake-Like Model of Supersonic Separated and Reattaching Turbulent Flows," AIAA Journal, Vol. 9, No. 4, Apr. 1971, pp. 703-712.

7. Raddatz, L. A., "The Douglas Aerophyics Laboratory Four-Foot Trisonic Wind Tunnel," DAC-59809, Douglas Aircraft Company, Santa Monica, California, Oct. 1967.

8. Roshko, A. and Thomke, G. J., "Observations of Turbulent Reattachment Behind an Axisymmetric Downstream-Facing Step in Supersonic Flow," AIAA Journal, Vol. 4, No. 6, June 1966, pp. 975-980.

9. Pate, S. R. and Schueler, C. J., "Effects of Radiated Aerodynamic Noise on Model Boundary-Layer Transition in Supersonic and Hypersonic Wind Tunnels," TR-67-236, USAF Arnold Engineering and Development Center, Tullahoma, Tennessee, Mar. 1968.

10. Hopkins, E. J., "Charts for Predicting Turbulent Skin Friction From the Van Driest Method (II)," TN D-6945, NASA Ames Research Center, Moffett Field, California, Oct. 1972.

11. Behrens, W., "Separation of a Supersonic Turbulent Boundary Layer by a Forward-Facing Step," Paper No. 71-127, AIAA 9th Aerospace Sciences Meeting, New York, Jan. 1971.

12. Zukoski, E. E., "Turbulent Boundary-Layer Separation in Front of a Forward-Facing Step," AIAA Journal, Vol. 5, No. 10, Oct. 1967, pp. 1746-1753.

13. Spaid, F. W. and Frishett, J. C., "Incipient Separation of a Supersonic, Turbulent Boundary Layer, Including Effects of Heat Transfer," AIAA Journal, Vol. 19, No. 7, July 1972, pp. 915-922.

14. Werle, M. J., "A Critical Review of Analytical Methods for Estimating Control Forces Produced by Secondary Injection," NOLTR 68-5, U.S. Naval Ordnance Laboratory, White Oak, Maryland, Jan. 1968.

15. Thomke, G. J. and Roshko, A., "Incipient Separation of a Turbulent Boundary Layer at High Reynolds Number in Two-Dimensional Supersonic Flow over a Compression Corner," DAC-59819, McDonnell Douglas Astronautics Company, Santa Monica, California, Jan. 1969.

16. Law, C. H., private communication, Aug. 1974.

17. Rose, W. C., Page, R. J. and Childs, M. E., "Incipient Separation Pressure Rise for a Mach 3.8 Turbulent Boundary Layer," AIAA Journal, Vol 11, No. 5, May 1973, pp. 761-763.

18. Rose, W. C., Murphy, J. D. and Watson, E. C., "Interaction of an Oblique Shock Wave with a Turbulent Boundary Layer," AIAA Journal, Vol. 6, No. 9, Sept. 1968, pp. 1792-1793.

19. Elfstrom, G. M., "Turbulent Hypersonic Flow at a Wedge-Compression Corner," J. Fluid Mech., Vol. 53, Part 1, Jan. 1972, pp. 113-127.

20. Sirieix, M., Délery, J. and Mirande, J., "Recherches Expériemntales Fondamentales Sur Les Écoulements Séparés et Applications," Le Recherche Aerospatiale, No. 520, 1967.

21. Appels, C., "Incipient Separation of a Compressible Turbulent Boundary Layer," Technical Note 99, von Karman Institute for Fluid Dynamics, Rhode-Saint Genese, Belgium, Apr. 1974.

22. Sterrett, J. R. and Emery, J. C., "Experimental Separation Studies for Two-Dimensional Wedges and Curved Surfaces at Mach Numbers of 4.8 to 6.2," TN-D-1014, NASA Langley Research Center, Langley Air Force Base, Va., Feb. 1962.

23. Holden, M. S., "Shock Wave-Turbulent Boundary Layer Interaction in Hypersonic Flow," AIAA Paper 72-74, Jan. 1972; also ARL 73-0137, Aerospace Research Laboratories, Wright-Patterson Air Force Base, Ohio, Oct. 1973.

24. Appels, C., "Turbulent Boundary Layer Separation at Mach12," Technical Note 90, von Karman Institute for Fluid Dynamics, Rhode-Saint Genese, Belgium, Sept. 1973.

25. Batham, J. P., "An Experimental Study of Turbulent Separating and Reattaching Flows at a High Mach Number," Journal of Fluid Mechanics, Vol. 52, Part 3, Apr. 1972, pp. 425-437.

26. Coleman, G. T. and Stollery, J. L., "Incipient Separation of Axially Symmetric Hypersonic Turbulent Boundary Layers," AIAA Journal, Vol. 12, No. 1, Jan. 1974, pp. 119-120.